Automated detection of illegal nonmetallic minerals mining places according to Sentinel-2 data

Usmanov, Bulat, Isakova, Liubov, Mukharamova, Svetlana, Akhmetzyanova, Leisan, Kuritsin, Ivan

Automated detection of illegal nonmetallic minerals mining places according to Sentinel-2 data

Liubov S. Isakova, Svetlana S. Mukharamova, Ivan N. Kuritsin,
Leisan G. Akhmetzyanova, Bulat M. Usmanov*
Institute of Environmental Sciences, Kazan Federal University, Kazan, Russia 420008

ABSTRACT

Currently, the problem of illegal mining is still acute. Such illegal use of natural resources harms the environment and leads to irrational use of mineral resources. Modern methods with the use of remote sensing technologies will effectively detect such law violations. In the current study, a method for automatically detection of non-metallic mineral extraction sites based on remote sensing data analysis has been developed. The study uses Sentinel-2 satellite images with spatial resolution 10 m and 20 m and considers four types of minerals: sand, clay, carbonate rocks and sand gravel mix. The spectral indices help to determine the specific quantitative characteristics of the mineral resources. The result is probability maps with mineral resources characteristics in each pixel. In order to determine to which of known classes relates the point, you need to find the covariance matrices for all classes and take the class with the smallest Mahalanobis distance to the point. Based on the obtained probability maps, an analysis of the applicability of the selected spectral indices was performed, as well as a visual assessment of the quality of interpretation. For each spectral channel and index, two frequency histograms were created to determine how different the channels values and spectral indices on the entire scene and at the reference objects. Each object found by the program was checked for it presence on the studied territory. The developed system is a modern, secure, non-contact method for the rational land use monitoring and natural resources extracted by open-pit mining study.

Keywords: remote sensing, mineral resources, illegal mining, spectral indices, R, natural resources management

1. INTRODUCTION

Open pit mining has a negative impact on the environment. As a result of anthropogenic impact on the environment in the area of the quarries, there is a noticeable deterioration of the ecological situation, for example, pollution of air, soil, bottom sediments, natural waters, as well as the impact on the flora and fauna[1,2]. However, today it is not possible to abandon the use of open mining. In addition to this, in Russia, there is still an acute problem of unauthorized mining, that is, mining without the required licenses. Therefore, it is necessary to carry out constant monitoring of the earth's surface in order to prevent violations of legislation in the field of mining and environmental protection. One of the operational and effective technologies for obtaining information about the properties and characteristics on the earth's surface is the remote sensing technology, which is especially important for our country due to its large area.

The purpose of the work is to assess the possibility of automated detection of unauthorized common minerals mining using Sentinel-2 satellite images. The relevance of the research topic is determined by the large number of objects of unauthorized mining in the territory of the Russian Federation, for which it is difficult to provide environmental monitoring by traditional methods. The methods used in the study can help automate the system for monitoring of the subsoil and unauthorized production sites state in large territories (regions, federal districts). Automation reduces the unauthorized quarries detection time and increases the monitoring area, which is important for the natural environment preservation.

1.1 Spectral indices overview

To work with spectral information, one often resorts to creating "index" images. Based on the combination of the brightness values in certain channels, which are informative for the selection of the object under study, and the calculation of the "spectral index" in each pixel, an image is built, which often helps to highlight the object under study or assess its state[3].

*busmanof@kpfu.ru

Soil reflectivity is the result of a combination of several factors such as particle size, soil structure, water content, surface roughness, organic matter content, minerals based on carbonates, quartz and iron oxide[4]. Each type of soil has a spectral characteristic according to the absorption of certain wavelengths of the electromagnetic spectrum[5,6]. Many soil types spectral indices have been developed from indices for detecting bare soils. The difficulty is that, for example, in agricultural areas it can be a natural state ("bare" soil), artificial (for example, construction) or crop rotation[7].

Piyoosh et al. provide an overview of the available indices for bare soils[8]. Many of them are specially created for mapping bare soil and settlements, since their spectral characteristics are quite similar. Vegetation indices also help deciphering soil types; combinations of NDVI and various indices for "bare" soils and buildings are often used[9,10,11,12,13].

The Normalized Difference Vegetation Index (***NDVI***) quantifies the presence of vegetation on the Earth's surface. It is the most common index for quantifying land cover problems[14].

The B8/B2 (R82) ratio of infrared to blue is a good indicator of the location of sand dune formation, helping to clearly differentiate sand from other materials. It was shown that the generated composite false color image, where the NIR/Blue ratio was used in the synthesis as red, NIR as green and Blue as blue, gave better recognition of active sand formations compared to the synthesis in natural colors. By classifying the image according to R82 using the quantile classification method, a threshold value was obtained in accordance with the distribution of sand in the desert (a value below the threshold meant that there was no sand on the selected surface)[15].

The Normalized Differential Sand Index (***NDSI***) was developed and used to monitor, map, and assess sand dune movement in parts of Iraq from 1988 to 2009. The index is calculated as the ratio of the measured intensities in the shortwave range. The calculated accuracy of the results of this study was 90.8%, which indicates the effectiveness of the created index, its high ability to decipher sand[16].

The Dry Bare Soil Index (***DBSI***) is used for decipher arid and semi-arid soils interpretation. It was created to find the difference between bare dry soil and buildings[17]. Based on a test performed on samples with bare soil pixels, a DBSI value of 0.26 and above was designated as bare soil, and areas with lower values - as other classes. Subtracting the NDVI in the DBSI index formula significantly improves the accuracy of the index and disambiguates in areas with high NDVIs (areas of high vegetation), which are often confused with built-up areas. The overall accuracy of the DBSI is 92%.

Supe et al. used the DBSI index for sand deposits detection on photovoltaic solar panels[18]. DBSI has a relatively higher potential (accuracy 89.6%, Kappa 0.77) in detecting of sand deposits in coparison to other indicators considered in the study. The combination of inputs such as DBSI together with NDSI also results in high performance of sand detection with 80% accuracy.

Two indices – Salt Minerals Index (***SMI***) and InfraRed Index-Short Wave InfraRed 1 (***IRI_SWIR1***) – are considered for the auxiliary decision tree classifier in order to build a land cover map for southeastern Tunisia[19]. The square root function has been used in SMI and IRI_SWIR1 to better differentiate areas with the same mineral content.

The Crust Index (***CI***) is based on the normalized difference between the red and blue spectra. CI is sensitive to soil characteristics, therefore it is able to detect various lithological and morphological units[20].

The Simple ratio Clay Index (***SRCI***) is defined as the ratio of the reflectance coefficients in two bands of the short-wave infrared range. Bousbih et al. was found that these spectral zones are most sensitive to clay content in dry seasons[21].

The Brightness Index (***BI***) combines information from the red and near infrared ranges. This index indicates the change in the average level of reflectivity. BI is often used to display soil characteristics such as roughness, texture, salinity and moisture. Dry soils with a low clay content tend to be highly reflective, while dark soils have low radiometric values in both bands due to high clay content. BI is used to find the difference between light and dark zones of soils, which correspond to sandy and clay soils[21].

The Normalized Difference Built-up Index (***NDBI***) detects urban areas and bare soils well by a sharp increase in reflectivity in the range from Red to SWIR1. This index is negative for water bodies, positive for urban areas and bare soil, and zero for forest and agricultural land[9].

Soil Adjusted Vegetation Index (***SAVI***) is a conversion method that minimizes the effects of soil brightness using red and near infrared wavelengths. When the index is equal to zero, it is considered as a bare soil indicator[22].

Bare Soil Index (**BSI**) – an index that combines 4 ranges to measure changes in soil properties[23]. This index is based on a combination of NDVI and NDBI[9]. The shortwave infrared and red spectral bands are used to quantify the mineral composition of the soil, the blue and near infrared spectral bands are used for better detection of vegetation. BSI has the lowest correlation with the NDVI index and the highest with DBSI[24]. High values of BSI and DBSI indices characterize bare soil, moderate values - built-up area, and low values - vegetation. BSI has been used in forest research to find the difference between bare soils and other land cover types[7,23,25], as well as for bare soil sites mapping and monitoring[13,26].

2. MATERIALS AND METHODS

2.1 Study area

Common nonmetallic minerals are the raw material base for the development of hydrocarbon production facilities, road construction and building materials production, therefore they are an important component of the Russia resource potential. The minerals considered in the work (sand, sand gravel mix, clays, carbonate rocks) are included in the list of common minerals of the Republic of Tatarstan (Russia).

The study considers the territory of the Republic of Tatarstan with an area of 100×100 km^2. Tatarstan is located in the center of the European part of Russia on the East European Plain, at the confluence of the two largest rivers – the Volga and the Kama. The territory of the republic stretches from west to east for 400 km, from north to south for 250 km and is a plain in the forest and forest-steppe zone with uplands. About 18% of the territory is covered with mixed forests. Tatarstan is rich in water resources. The soils are very diverse – from gray forest and podzolic soils in the north and west to various types of chernozems in the south of the republic[27].

The choice of the territory is due to the availability of ground data, as well as one of the scenes (39UVB) of the Sentinel-2 satellite data. We used Sentinel-2 images of the second processing level (Level-2A) on 06/21/2019 and 09/12/2019. Data on a number of mining sites for nonmetallic minerals were obtained as a result of field studies in 2019 and are presented in the form of a table indicating the type of mined raw materials, approximate coordinates, description of the geographical location for each quarry.

2.2 Pre-processing

For each of the 2 images, using the utilities of the GDAL library, all channels were brought to the best resolution (10 m) and saved into the one GeoTiff file. Further, for each image, 12 raster layers were calculated with the values of the spectral indices presented in Table 1. As a result, two composites were constructed – for 06/21/2019 and for 09/12/2019, consisting of 22 layers: 10 channels and 12 spectral indices.

2.3 Training samples creation

To apply recognition algorithms (supervised classification, supervised classification), it is necessary to have a training sample for each type of target objects (quarries). Based on the training sample, the recognition algorithms are tuned, therefore the quality of the formed sample is critical for successful recognition.

To create training samples for 4 types of materials (sand, sand gravel mix, clays, carbonate rocks), field observations data of 2019 were used. On these data, a vector layer was created with reference quarry locations - 31 polygonal objects.

Further, for the pixels corresponding to the reference locations of various types of quarries, values were obtained in 22 channels for each of the 2 analyzed composites. For processing, a program was written in the R language[28]. At the output, the program creates a text file for each composite containing a multidimensional sample, were lines correspond to pixels. Minerals type, reflection coefficients values in 10 spectral channels and 12 spectral indices values are given for each pixel (Table 1). In total, 8 training samples were formed – for 4 types of quarries based on 2 Sentinel-2 satellite data composites.

2.4 Mahalanobis distance classification

To solve the main task of the work, the methods of supervised classification (classification with a teacher) were applied. Our task is a special case of classification, one of the main problems in images interpretation – the search for objects in the presence of only "positive" information, that is, only data on the locations of the target object or phenomenon. This problem is solved using the similarity of spectral characteristics either by empirical methods (such as the nearest neighbor method), or by purely parametric methods, when the brightness probability distribution in the phenomenon placement is known. Two supervised classification methods were used to detect mining sites using Sentinel-2 data: the Mahalanobis distance and the maximum entropy.

Table 1. Spectral indices.

Index	Index formula	Index formula in the spectral channels Sentinel-2 notation
NDVI	$\dfrac{NIR - Red}{NIR + Red}$	$\dfrac{b8 - b4}{b8 + b4}$
R82	$\dfrac{NIR}{Blue}$	$\dfrac{b8}{b2}$
NDSI	$\dfrac{SWIR2 - Red}{SWIR2 + Red}$	$\dfrac{b12 - b4}{b12 + b4}$
DBSI	$\dfrac{SWIR1 - Green}{SWIR1 + Green} - NDVI$	$\dfrac{b11 - b3}{b11 + b3} - \dfrac{b8 - b4}{b8 + b4}$
SMI	$\sqrt{\dfrac{Blue^2 + Green^2 + Red^2}{SWIR2}}$	$\sqrt{\dfrac{b2^2 + b3^2 + b4^2}{b12}}$
IRI_SWIR1	$\sqrt{\dfrac{NIR^2 + SWIR2^2}{SWIR1}}$	$\sqrt{\dfrac{b8^2 + b12^2}{b11}}$
CI	$1 - \dfrac{Red - Blue}{Red + Blue}$	$1 - \dfrac{b4 - b2}{b4 + b2}$
SRCI	$\dfrac{SWIR1}{SWIR2}$	$\dfrac{b11}{b12}$
BI	$\sqrt{Red^2 + NIR^2}$	$\sqrt{b4^2 + b8^2}$
NDBI	$\dfrac{SWIR1 - NIR}{SWIR1 + NIR}$	$\dfrac{b11 - b8}{b11 + b8}$
SAVI	$\dfrac{(1 + 0,5) \cdot (NIR - Red)}{NIR + Red + 0,5}$	$\dfrac{(1 + 0,5) \cdot (b8 - b4)}{b8 + b4 + 0,5}$
BSI	$\dfrac{(Red + SWIR1) - (NIR + Blue)}{(Red + SWIR1) + (NIR + Blue)}$	$\dfrac{(b4 + b11) - (b8 + b2)}{(b4 + b11) + (b8 + b2)}$

The Mahalanobis distance method is used when spectral features of different classes can be similar and their brightness ranges overlap. According to the decision rule, a pixel belongs to the reference class, the distance of Mahalanobis to the center of which in the feature space is minimal. In our case, with one-class classification (detection), the Mahalanobis distance is recalculated into the probability of a pixel belonging to a class using the chi-square distribution.

This method was implemented using a program written in the R language. The program for a fixed type of quarry at the first step calculates the mean vector μ and the covariance matrix COV using the corresponding training sample. Then it loads the prepared composite and in each pixel calculates the Mahalanobis distance to the training set, recalculating it into the probability of the pixel belonging to the detected type of quarry.

As a result, for each of the 2 composites, 4 raster files were created, in the pixels of which the values of the probability of the sand, sand gravel mix, clay, carbonate rocks quarry presence are recorded, respectively.

2.5 Classification by the maximum entropy method

The result of the maximum entropy method is not just a classifying solution, but a probability value for a given class. The set of weights α is found by numerical optimization using training data[29,30]. To apply the maximum entropy method, we used the MaxEnt program[31]. This software was developed to simulate ecological niches and the distribution of plant species in the study area. This machine learning algorithm predicts the presence of a species in a geographic space based only on the points where the species was observed, excluding the locations of its documented absence[32]. Based on the analysis of a set of georeferenced observation sites of a particular type (a list of coordinates of points where the presence

of a species is marked) and a set of raster layers with environmental factors (for example, temperature, precipitation, soil properties, etc.), the program creates, using the maximum entropy method, a model of distribution of probabilities of a given species presence. The program also generates a raster layer, where each terrain cell has the predicted suitability of conditions for the species. A high capability value in a particular grid cell indicates suitable conditions for that species. We are looking for locations with spectral characteristics similar to those of the "training" quarry sites. In our case, a set of georeferenced quarries of a specific type of minerals (locations from the corresponding training sample) and a set of satellite data raster layers (10 spectral channels and 12 spectral indices) are analyzed for the study area.

3. RESULTS AND DISCUSSION

3.1 Analysis of target objects spectral properties

The spectral properties of the recognized objects were studied based on training samples. For this purpose, the graphs of the spectral curves were built. For each of the 2 images taken on different dates, the reflectance values in 10 spectral channels (Sentinel 2) in pixels with a fixed type of quarry were summarized using the average and displayed on graphs (Fig. 1).
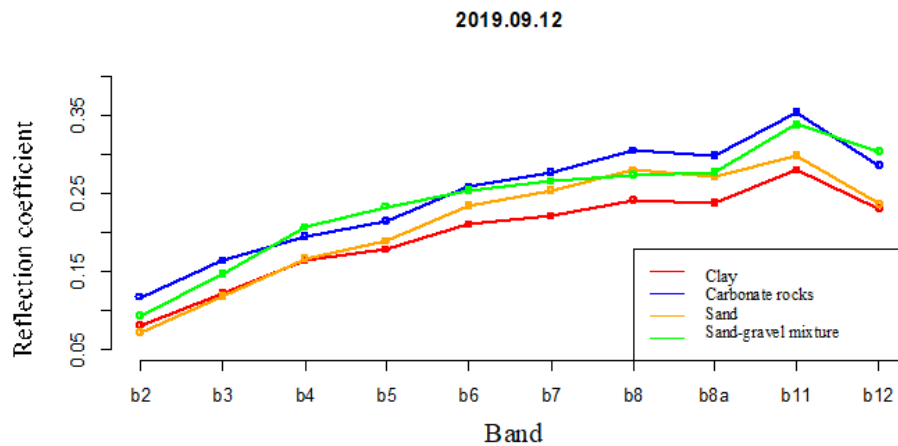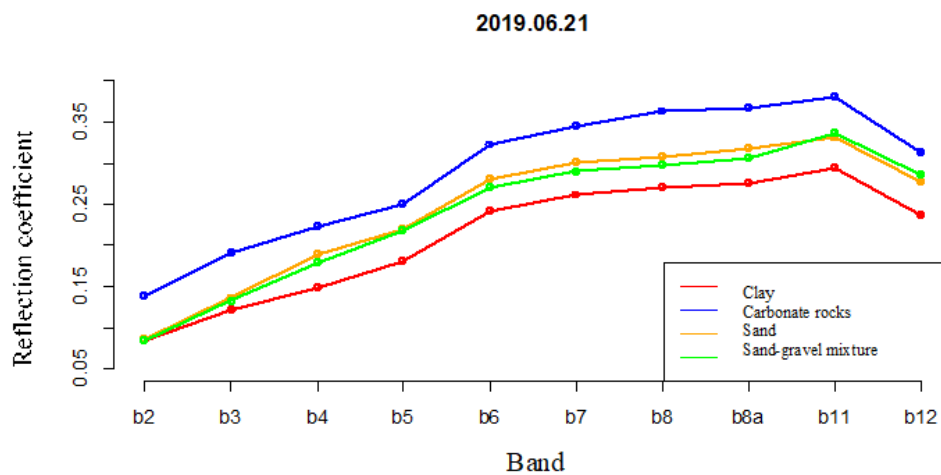
Figure 1. Reflectance values in 10 spectral channels of the Sentinel 2.

The resulting graphs show the spectral features of different types of mined materials: sand, sand gravel mix, clay, carbonate rocks. It can be seen that for all analyzed materials, the reflectivity increases with increasing wavelength. At the same time, the reflection coefficients in all channels of the June image for sand and sand gravel mix are practically equal. In the same image, the reflectivity of carbonate rocks exceeds that of other materials over the entire spectral range.

In the September image, the reflectance values of clay and sand in the blue, green and red channels are nearly identical, as are sand gravel in the near infrared (b8) and narrow near infrared (b8A). Similar to the June image, clay has the lowest reflection coefficients in all channels, and carbonate rocks have the highest, almost everywhere. Comparing the two graphs, it can be seen that the reflectivity of all 4 types of minerals is higher in June. Differences between reflectivity are also more pronounced in the June graph (except for sand and sand gravel mix), while in the September graph the spectral curves are close and often intersect.

The spectral indices of the analyzed object types have rather close values, especially the SAVI and SRCI indices in the June image and the NDSI in the September image. The most contrasting difference was shown by the R82 index. Its highest values have a sand gravel mix in June and sand in September. The values of the DBSI and CI indices are equally ranked by mineral type in both images. According to the BI values, it is noticeable that the texture, salinity and moisture content of the studied minerals have more similar states in the autumn period.

Spectral plots of 4 types of minerals indicate the difficulty of recognizing them by remote sensing data, due to the similarity of their spectral properties, which can lead to an incorrect decision about the type of detected material. Moreover, it is a priori clear that the spectral properties of target objects are not specific enough. They are quite similar not only to each other, but also to the properties of a number of other types of surface in the study area, for example, open ground, some open soils (without vegetation) etc. To understand the measure of their specificity, frequency histograms of values in pixels of the entire territory and training samples (within the boundaries of reference polygons) were constructed. Histograms for the sand gravel mix are shown in Fig. 2-3. Next, the "separability" of the histograms was visually analyzed for each spectral channel and each index.
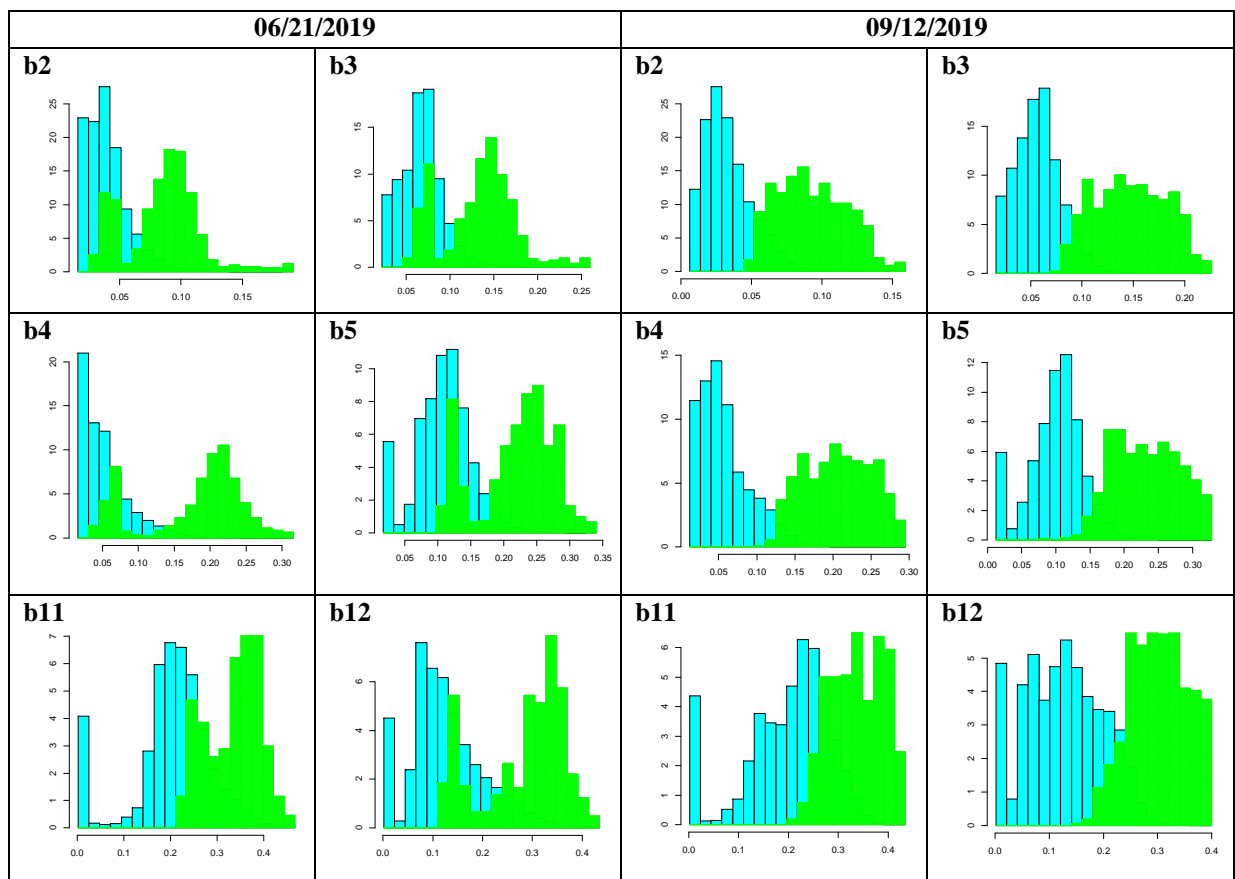

Figure 2. Frequency histograms of the spectral channels values for the entire territory (blue) and for the training sample (green), sand gravel mix.
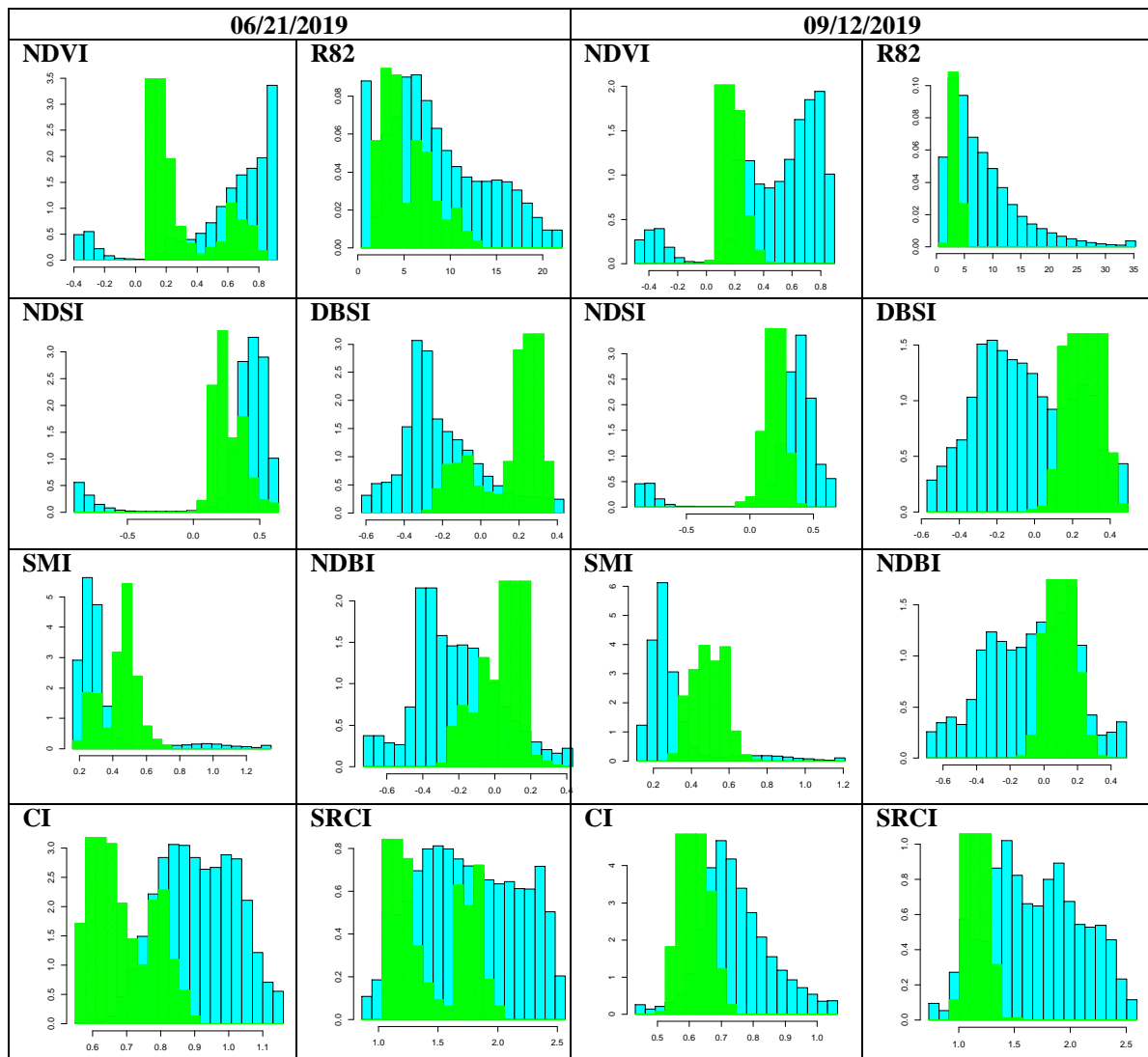
Figure 3. Frequency histograms of the spectral indicies values for the entire territory (blue) and for training sample (green), sand gravel mix

The analysis showed that for sand and sand gravel mix, both in June and September, the greatest difference from the background values is observed in channels b2, b3, b4, b12 (the difference is more contrast in the June image), slightly less in channels b5, b11. The histograms for near infrared channels b6, b7, b8, b8a do not show separability. There is no separability for BI, NDBI, SRCI, IRI indices or it is bad both in June and in September. BSI, DBSI, SAVI, CI and R82 have bad indexes in September, better in June. Indices NDVI, NDSI, SMI, DBSI (June), SAVI (June, sand gravel mix) showed the best difference between their values in pixels of sand and sand and gravel mix from the background.

Histograms for clay and carbonate rocks show similar specificity for both channel values and indices. The best separability for clay is observed in channel b4. Carbonate rocks, unlike other types, have practically the same histograms of values in spectral channels in summer and autumn. In addition, the separability of histograms for carbonate rocks in the channels of the visible spectrum zone (b2, b3, b4) is higher than for other types.

3.2 Analysis of the spectral indices applicability for quarries recognition

Histograms for various types of minerals showed that there is not a single spectral index clearly separating the frequencies of values for the entire territory and for training samples. The frequency histograms are superimposed on each other, therefore, the intersection interval contains both the values of the target objects (minerals quarries), and other types of land cover in the study area. It may also be objects that are not included in the training sample (those that are to be detected), but their part is deliberately extremely small for a territory of this size.

To assess the suitability of spectral indices for recognition purposes, a threshold classification was applied. As an example, the results (06.21.2019) of the DBSI spectral index (best histograms separability) evaluation for sand recognition are given (Fig. 4). When building maps, thresholds are set in the gradient palette based on histogram values. Recognition results are displayed in red. It can be seen that, in addition to the training quarries, too many false detection sites were identified. On the right in Figure 4, fragments are shown that demonstrate an index response on a training sample object (above) and one of the many false positives (below).
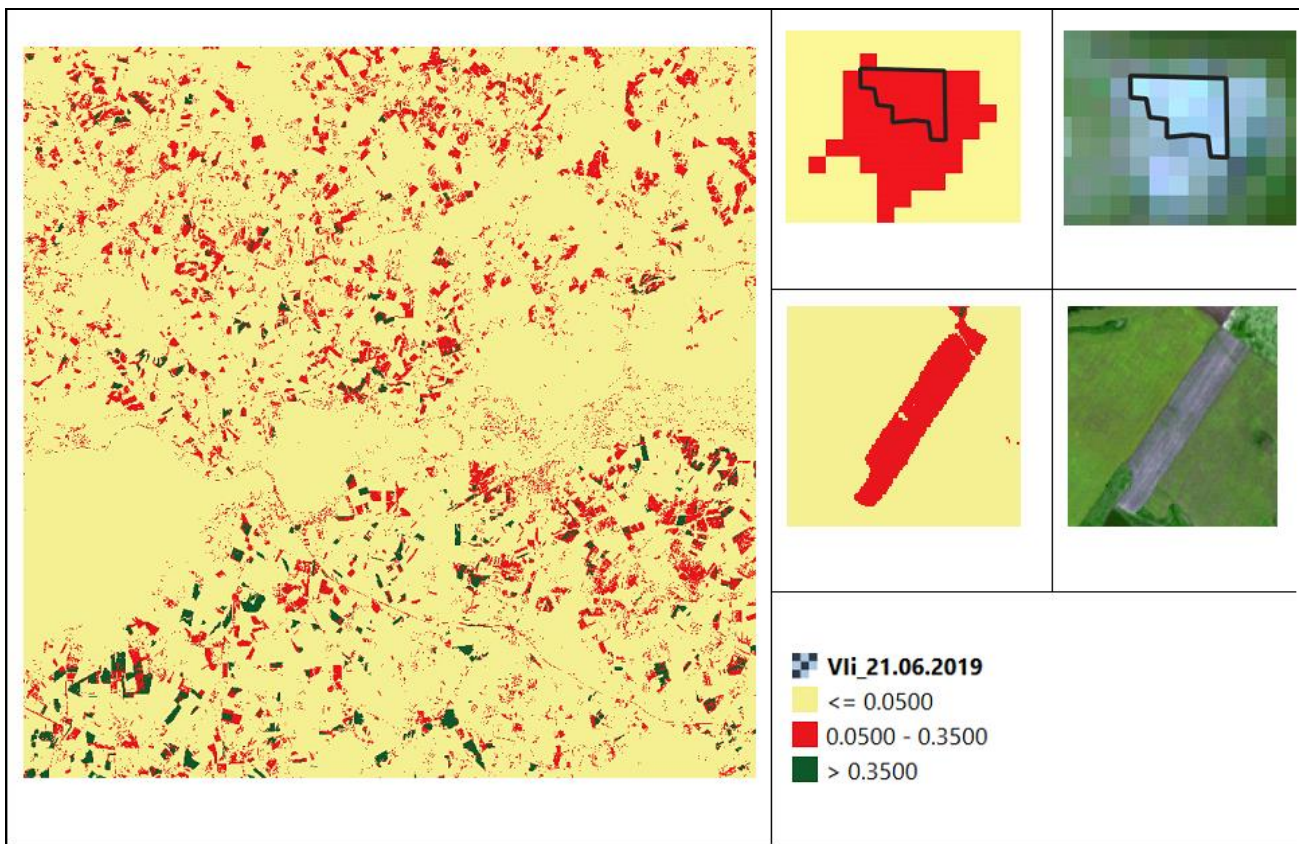
Figure 4. Gradient map of the DBSI index (06/21/2019). Examples of correct (top right) and false (bottom right) quarry recognition.

Based on the results of the analysis, it can be concluded that the spectral indices taken separately do not have the required sensitivity and do not provide an adequate estimate of the location of the minerals quarries. Experiments have shown that the simultaneous use of two or more indices gives a slightly better result. After a series of experiments in order to increase the detection efficiency, we decided to use a composite for quarry recognition, which includes as the initial spectral information - 10 image channels as well 12 spectral indices.

3.3 Assessing the contribution of input variables to forecasting.

In our case, a set of georeferenced quarries of certain minerals (reference locations from the corresponding training sample) and a set of satellite raster layers (10 spectral channels and 12 spectral indices) are analyzed.

Composite 10 channels and 12 spectral indices were loaded in the MaxEnt parameters section with information about the environment. In the "samples" section – a file with sample quarries coordinates.

As a result, for each of the 2 composites (June 21, 2019 and September 12, 2019), probability distribution models were obtained for each type of quarry (a total of 8 rasters) with detailed reports containing statistical analysis of accuracy, an estimate of the input variables contribution to forecasting. According to MaxEnt estimates, the following spectral variables made the most significant contribution to forecasting for different types of quarries (Table 2).

Table 2. Contribution of spectral variables to forecasting the types of quarries (in descending order of contribution).

Quarry type	06/21/2019	09/12/2019
Sand	b4, CI, NDSI	b4, CI, NDBI
Sand gravel mix	b4, CI, b2	b4
Clay	b4, NDVI, NDSI	b4, b11, NDSI
Carbonate rocks	b4, SMI	b2, b4, b3

These results are consistent with the histograms analysis. It can be noted that the greatest contribution to recognition is made by the spectral data of the red spectrum range (b4).

3.4 Recognition quality assessment.

After obtaining the resulting rasters with the quarries probabilities, our task is to understand whether the technology being developed is working well. To assess the recognition quality, ground data and the recognition result are compared. Both reference objects of the training sample and the data of an independent (not involved in training) control sample can be used. Errors and indicators of recognition accuracy are calculated (commission, commission, user accuracy, manufacturer accuracy, etc.). That is, they quantify how well objects of a given type are detected: the percentage of correctly recognized, not recognized, falsely recognized, etc.

In our case, the training sample is too small, and it was not possible to divide it into two parts - for training and for control. Therefore, the quantitative indicators of the recognition quality were evaluated on reference objects, including using cross-validation for MaxEnt. The values of errors depend on the probability threshold value for decision making: the probability in a pixel is below the threshold – there is no target object, above – there is an object. The higher the threshold value – more gaps, the less – more false positives. Fig. 5 shows the values of the ommision errors (missing targets, blue) and the predicted area (proportion of the study territory area, red) depending on the threshold value (probability, in%) for recognition by the MaxEnt method.

Analysis of MaxEnt errors was carried out using ROC curves (Fig. 6). Since we only have find data, but no missing data, a fractional predicted area is used instead of a commission error.

The closer the red line is to the upper left corner, the better the classifier predicts the reference objects. The quantitative interpretation of ROC is given by the AUC (area under curve) indicator. The higher the AUC, the better the classifier. Using only individual spectral indices results in too many false positives. The result is significantly better when using all spectral information (composite).

A separate task was to detect quarries that were not included in the training sample. Since there are not so many pixels with a nonzero probability on the resulting rasters, a visual assessment of the recognition adequacy is possible. For this, an RGB image was synthesized using the Sentinel-2 channels (b4, b3, b2), and a raster of probability (for example, sand) was displayed in the gradient palette. The final quality assessment was carried out using detailed Google or Yandex satellite images. In the study area, 25 "new" quarries were found that did not belong to the training sample. Below in some of the results are shown (Table 3), allowing to draw a conclusion about the efficiency of the developed technology.

Comparison of the recognition results obtained by different methods (Mahalanobis distance and the method of maximum entropy) did not show the advantages of a particular method. Recognition from summer (June 21, 2019) and autumn (September 12, 2019) images also gave comparable accuracy of the results.
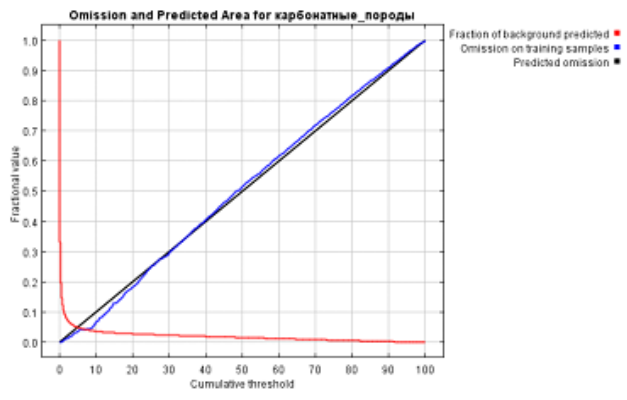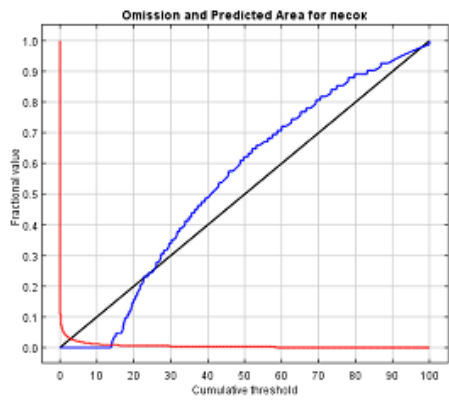
Figure 5. Ommission errors for sand (left) and carbonate rocks (right) by remote sensing data (06/21/2019).
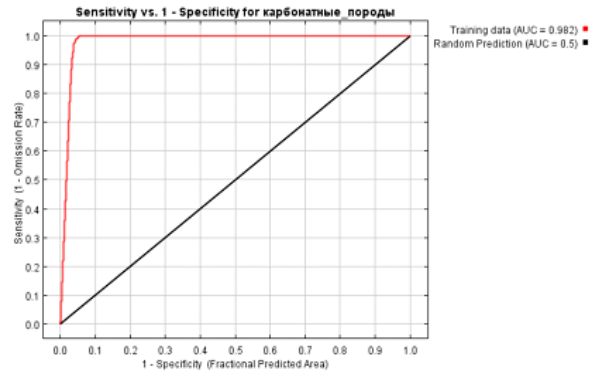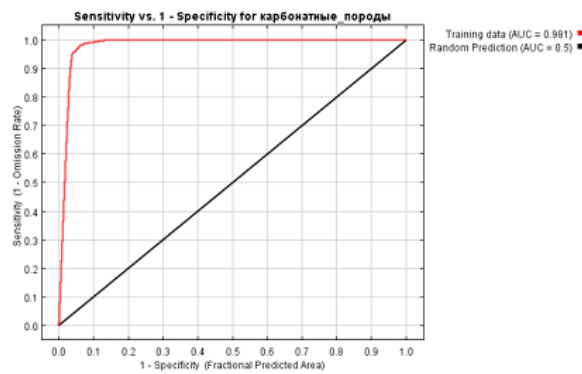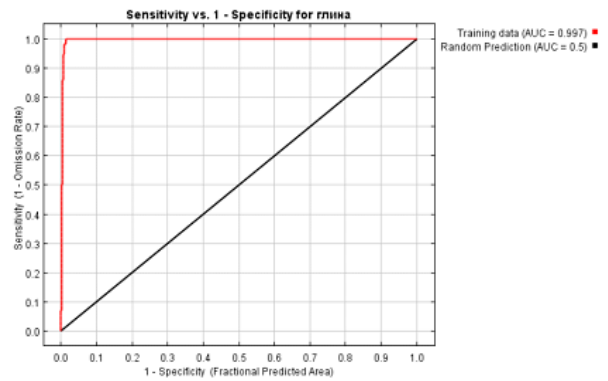

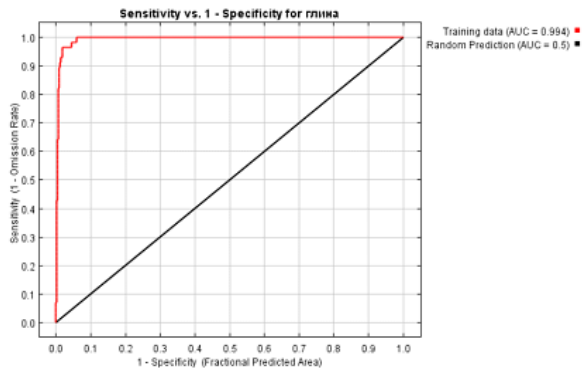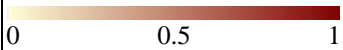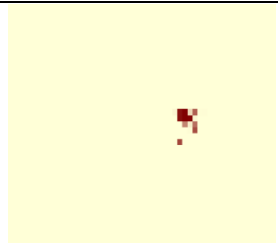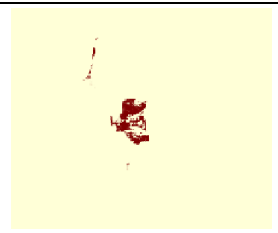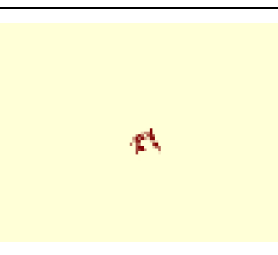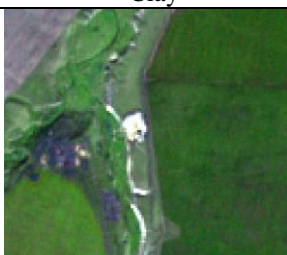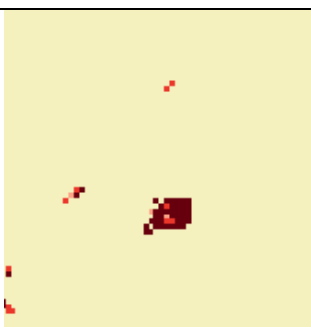Figure 6. ROC curves for clay and carbonate rock quarries recognition by the MaxEnt method by remote sensing data (06/21/2019 (left) and 09/12/2019 (right)).

Table 3. Quarry locations assessment

Quarry probability 0 0.5 1	Sentinel-2 RGB composite	Google/Bing/Yandex image
Sand		
Sand gravel mix		
Clay		
Carbonate rocks		

4. CONCLUSION

Based on the results of the study, the following conclusions can be drawn:

−   Separately, spectral indices cannot effectively predict the locations of mineral quarries. Composites of multiple indexes must be used.

−   The red spectrum range makes the greatest contribution to recognition. Spectral channels and indices composite allow minimizing of false positives during recognition.

−   Satellite images seasonality (summer-autumn) does not significantly affect the accuracy of quarries detection.

– Despite the fact that the spectral properties of the studied types of quarries are not specific enough and are similar to the properties of a number of other objects in the study area, the recognition quality using the developed technology can be considered quite acceptable, especially taking into account the area of the studied territory and the specific sizes of the detected objects.

– Information on the discovered quarries coordinates allows the interested organizations to either carry out an on-site or in permits register check for unauthorized development of minerals.

The introduction of the applied methods will create a modern science-based approach to the detection of unauthorized common minerals extraction places by the supervisory authorities.

ACKNOWLEDGEMENTS

REFERENCES

[1] Yermolaev, O.P., Usmanov, B.M. and Muharamova, S.S., "The basin approach and mapping to the anthropogenic impact assessment on the east of the russian plain," International Journal of Applied Engineering Research Papers 10 (20), 41178-41184 (2015).

[2] Yermolaev, O. and Usmanov, B., "The Basin Approach to the Anthropogenic Impact Assessment in Oil-Producing Region," Proc. 14th International Multidisciplinary Scientific Geoconference SGEM, 681-688 (2014).

[3] Cherepanov, A.S. and Druzhynina, Y.G., "Spectral properties of vegetation and vegetation indices" Geomatics Papers 2, 28-32 (2009). (in Russian)

[4] Dematte, J. A. M., Galdos M. V., Guimarães R. V., Genú A. M., Nanni M. R. and Zullo Jr J., "Quantification of tropical soil attributes from ETM+/LANDSAT-7 data," Int. J. Remote Sens. Papers 28(13), 3813-3829 (2007).

[5] Vasyukov, S.V., Sirotkin, V.V. and Usmanov, B.M., "Spectrometric characteristics of soils of the subboreal zone of the eastern part of the Russian plain," Proc. SPIE 11524, Eighth International Conference on Remote Sensing and Geoinformation of the Environment (RSCy2020), 1152406 (2020).

[6] Sirotkin, V., Vasyukov, S. and Usmanov B., "The possibility of using spectrographic data to assess soils fertility," International Multidisciplinary Scientific GeoConference Surveying Geology and Mining Ecology Management, SGEM 17(32), 639-646 (2017). DOI: 10.5593/sgem2017/32/S13.083

[7] Diek, S., Fornallaz, F., Schaepman, M. E. and Jong, R.D., "Barest Pixel Composite for Agricultural Areas Using Landsat Time Series," Remote Sensing Papers 9(12), 1245 (2017).

[8] Piyoosh, A.K. and Ghosh, S.K., "Development of a modified bare-soil and urban index for Landsat 8 satellite data," Geocarto Int. Papers 33(4), 1-20 (2017).

[9] Zha, Y., Gao, J. and Ni, S., "Use of normalized difference built-up index in automatically mapping urban areas from TM imagery," Int. J. Remote Sens. Papers 24, 583-594 (2003).

[10] He, C., Shi, P., Xie, D. and Zhao, Y., "Improving the normalized difference built-up index to map urban built-up areas using a semiautomatic segmentation approach," Remote Sens. Lett. Papers 1, 213-221 (2010).

[11] Stathakis, D., Perakis, K. and Savin, I., "Efficient segmentation of urban areas by the VIBI," Int. J. Remote Sens. Papers 33, 6361-6377 (2012).

[12] Rikimaru, A., Roy, P.S. and Miyatake, S., "Tropical forest cover density mapping," Trop. Ecol. Papers 43, 39-47 (2002).

[13] Chen, W., Liu L., Zhang, C., Wang J., Wang J. and Pan Y., "Monitoring the seasonal bare soil areas in beijing using multi-temporal TM images," Proc. IEEE Int. Geoscience and Remote Sens. Symp., 3379-3382 (2004).

[14] Kriegler, F.J., Malila, W.A., Nalepka, R.F., Richardson, W., "Preprocessing transformations and their effects on multispectral recognition," Proc. Sixth Int. Symp. Remote Sensing of Env. 97, 131 (1969).

[15] Gomez, D., Salvador, P., Sanz, J., Casanova, C. and Casanova, J. L., "Detecting Areas Vulnerable to Sand Encroachment Using Remote Sensing and GIS Techniques in Nouakchott, Mauritania," Remote Sens. Papers 10(1541), 2-18 (2018).

[16] Al-Quraishi Ayad, M. F., "Sand dunes monitoring using remote sensing and GIS techniques for some sites in Iraq," Proc. SPIE 8762, 876206 1-9 (2013).

[17] Rasul, A., Balzter, H., Ibrahim, G.R.F., Hameed, H.M., Wheeler, J., Adamu, B., Ibrahim, S. and Najmaddin, P.M., "Applying Built-Up and Bare-Soil Indices from Landsat 8 to Cities in Dry Climates," Land Papers 7(3), 2-13 (2018).

[18] Supe, H., Avtar, R., Singh, D., Gupta, A., Yunus, A.P., Dou, J., Ravankar, A.A., Mohan, G., Chapagain, S.K., Sharma, V., Singh, C.K., Tutubalina, O. and Kharrazi, A., "Google Earth Engine for the Detection of Soiling on Photovoltaic Solar Panels in Arid Environments," Remote Sens. Papers 1466 (2020).

[19] Afrasinei, G.M., Melis, M.T., Arras, C. and Pistis M., "Spatiotemporal and spectral analysis of sand encroachment dynamics in southern Tunisia," European J. Remote Sens. Papers 51(1), 352-374 (2018).

[20] Pandey, P.C., Rani, M., Srivastava, P.K., Sharma, L.K. and Nathawat, M.S., "Land degradation severity assessment with sand encroachment in an ecologically fragile arid environment: a geospatial perspective," Qscience Connect Papers 43, 2-17 (2013).

[21] Bousbih, S., Zribi, M., Pelletier, C., Gorrab, A., Lili-Chabaane, Z., Baghdadi, N., Aissa, N.B. and Mougenot, B., "Soil Texture Estimation Using Radar and Optical Data from Sentinel-1 and Sentinel-2," Remote Sens. Papers 11(13), 1520 (2019).

[22] Huete, A.R., "A soil-adjusted vegetation index (SAVI)," Remote Sensing of Environment, 295-309 (1988).

[23] Rikimaru, A., Roy, P.S. and Miyatake, S., "Tropical forest cover density mapping," Trop. Ecol. Papers 43, 39-47 (2002).

[24] Rouibah, K. and Belabbas, M., "Applying Multi-Index Approach from Sentinel-2 Imagery to Extract Urban Areas in Dry Sea son (Semi-Arid Land in North East Algeria)," Revista de Teledeteccion Papers 56, 89-101 (2020).

[25] Jamalabad, M. and Abkar, A.A., "Forest canopy density monitoring, using satellite images," Proc. Geo-Imagery Bridging Continents XXth ISPRS Congress, 12-23 (2004).

[26] Zhao, H. and Chen, X., "Use of normalized difference bareness index in quickly mapping bare areas from TM/ETM+," Proc. IEEE Int. Geoscience and Remote Sens. Symp., Seoul, 1666-1668 (2005).

[27] Gaysin, I.T., Khusainov, Z.A. and Galimov, Sh., "Geography and ecology of the Republic of Tatarstan," KGPU Publishers, Kazan, 150-204 (2003). (in Russian)

[28] Akhmetzyanova, L.G., Saveliev, A.A. and Selivanovskaya, S.Y., "Using the methods of statistical analysis to determine the safe content of oil products in gray forest soil," Contemporary Problems of Ecology Papers 5(6), 554-558 (2012).

[29] Phillips, S.J. and Dudik, M., "Modeling of Species Distributions with MaxEnt: New Extensions and a Comprehensive Evaluation," Ecography Papers 31, 161-175 (2008).

[30] Merow, C., Smith, M.J. and Silander, Jr J.A., "A practical guide to MaxEnt for modeling species' distributions: what it does, and why inputs and settings matter," Ecography Papers 36, 10, 1058-1069 (2013).

[31] Phillips, S. J., Dudík, M. and Schapire, R.E., "Maxent software for modeling species niches and distributions," (Version 3.4.3), (2021).

[32] Lisovsky, A.A. and Dudov, S.V., "Advantages and limitations of methods of ecological modeling of habitats. 2. Maxent.," Journal of General Biology Papers 81(2), 135-146 (2020). (in Russian)